A New Approach to Sensorless Control Method for Brushless DC Motors

Tae-Sung Kim, Byoung-Gun Park, Dong-Myung Lee, Ji-Su Ryu, and Dong-Seok Hyun

Abstract: This paper proposes a new position sensorless drive for brushless DC (BLDC) motors. Typical sensorless control methods such as the scheme with the back-EMF detection method show high performance only at a high speed range because the magnitude of the back-EMF is dependent upon the rotor speed. This paper presents a new solution that estimates the rotor position by using an unknown input observer over a full speed range. In the proposed method, a trapezoidal back-EMF is modelled as an unknown input and the proposed unknown input observer estimating a line-to-line back-EMF in real time makes it possible to detect the rotor position. In particular, this observer has high performance at a low speed range in that the information of a rotor position is calculated independently of the rotor speed without an additional circuit or complicated operation process. Simulations and experiments have been carried out for the verification of the proposed control scheme.

Keywords: BLDC motor, full speed range, sensorless control, unknown input observer.

1. INTRODUCTION

Brushless DC (BLDC) motors have the advantage of higher power density than other motors such as induction motors because of having no copper losses on the rotor side and they do not need mechanical commutation mechanisms as compared with DC motors, which results in compact and robust structures. Owing to these features, BLDC motors have become more popular in the applications where efficiency is a critical issue, or where spikes caused by mechanical commutation are not allowed. A BLDC motor requires an inverter and a rotor position sensor to perform commutation process because a permanent magnet synchronous motor does not have brushes and commutators in DC motors. However, the position sensor presents several disadvantages from the standpoints of drive's cost, machine size, reliability, and noise immunity. As a result, many researches have been reported for sensorless drives that can control position, speed, and/or torque without shaft-mounted position sensors [1,2].

Conventional sensorless control methods can be classified into four categories. First, the open phase current sensing method [3] is a technique for detecting the conducting interval of freewheeling diodes connected in antiparallel with power transistors. It has the advantage that the synchronous process is simple and the control characteristic has high performance at low speeds. However, rotor position resolution conspicuously decreases at high speeds. In particular, for realization of this method, it has the defect that additional isolated power needs to supply to a comparator for detecting the freewheeling current. Secondly, the method detecting the third harmonic of back-EMF [4,5] is the technique to remove all the fundamental and other polyphase components through a simple summation of three phase voltages. There is a reduced filtering requirement for the integration function performed on a signal, which has a frequency three times that of the fundamental signal. Eventually, the filter has a much smaller capacity than the flux detection method using back-EMF, it is not sensitive to filtering delays and achieves high performance over a wide speed range. However, a neutral point that is not considered in the manufacturing process of the motor is required to measure phase voltages. Also, the third harmonics detection is difficult at a low speed range. Thirdly, the back-EMF integrating method [6,7] is a technique applying the principle that integration is constant from Zero Crossing Point (ZCP) to 30°. There is the advantage that the operation of the main processor decreases, seeing that it is not necessary to calculate an additional conversion point of the switching mode. This method does not synchronize the phase current with the back-EMF at the sensorless

Manuscript received February 29, 2008; accepted May 28, 2008. Recommended by Geust Editor Seung Ki Sul.

Tae-Sung Kim, Byoung-Gun Park, and Dong-Seok Hyun are with the School of Electrical Engineering, Hanyang University, 17 Haengdang-dong, Seongdong-gu, Seoul 133-791, Korea (e-mails: {redtea, redalarm, dshyun}@hanyang.ac.kr).

Dong-Myung Lee is with the School of Electronics and Electrical Engineering, Hongik University, 72-1, Sangsu-dong, Mapo-gu, Seoul 121-791, Korea (e-mail: dmlee@hongik.ac.kr).

Ji-Su Ryu is with the Company of Hanyoung Electrical Industry Galjeon-ri, Miyang-myeon, Anseong-Si, Gyeonggi-do 228-16, Korea (e-mail: jsryu0@empal.com).

drive. Besides, the flux-weakening drive is impossible. Finally, the open phase voltage sensing method [8-11] is a scheme estimating the rotor position indirectly by using the ZCP detection of open phase's terminal voltage. It is the most commonly used sensorless control method. However, this method has a deteriorated response at transient state and requires high operational speed enough to detect the ZCP of terminal voltages.

To solve above problems, this paper proposes a new sensorless control method utilizing an unknown input observer. The unknown input observer has been widely researched [12-14], especially in the fault detection field [15-17]. However, this observer has not been adopted in sensorless BLDC motor control application. Hence, this paper presents a new sensorless control method incorporating an unknown input observer that is independent of the rotor speed for a BLDC motor drive. As a result, this paper proposes a highly useful new solution for a sensorless BLDC motor drive, which can effectively estimate a line-to-line back-EMF.

2. MODELLING OF BLDC MOTORS

The BLDC motor drive block diagram is shown in Fig. 1.

Assuming that the stator resistances of all the windings are equal, and also self and mutual inductances are constant, the voltage equation of the three phases can be expressed as (1) [18]. In this equation, magnets, stainless steel retaining sleeves with high resistivity, and rotor-induced currents are neglected and no damper windings are modelled.

$$\begin{bmatrix} v_a \\ v_b \\ v_c \end{bmatrix} = \begin{bmatrix} R_s & 0 & 0 \\ 0 & R_s & 0 \\ 0 & 0 & R_s \end{bmatrix} \begin{bmatrix} i_a \\ i_b \\ i_c \end{bmatrix} + \begin{bmatrix} L_s - M & 0 & 0 \\ 0 & L_s - M & 0 \\ 0 & 0 & L_s - M \end{bmatrix} \frac{d}{dt} \begin{bmatrix} i_a \\ i_b \\ i_c \end{bmatrix} + \begin{bmatrix} e_a \\ e_b \\ e_c \end{bmatrix} \tag{1}$$

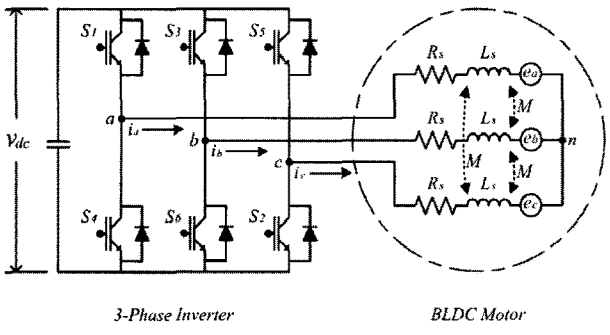

Fig. 1. Block diagram of a BLDC motor drive.

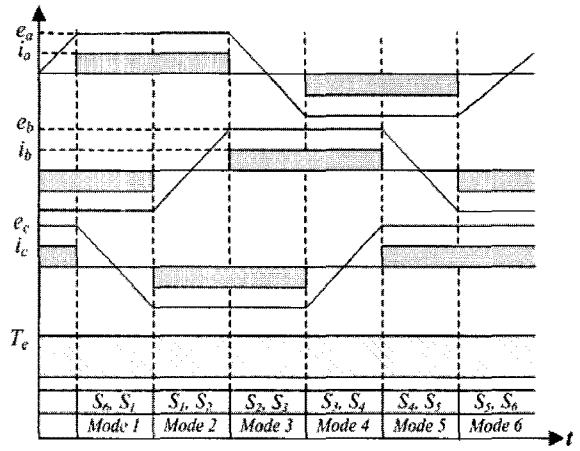

Fig. 2. Waveforms of a back-EMF, a phase current and a torque of BLDC motor.

The torque equation is given by:

$$T_e = \frac{e_a \cdot i_a + e_b \cdot i_b + e_c \cdot i_c}{\omega_m}, \tag{2}$$

where v_a, v_b, and v_c are phase voltages. R_s is a stator resistance. i_a, i_b, and i_c are phase currents. L_s is a stator inductance. M is a mutual inductance. Where, hereinafter L represents $L_s - M$. e_a, e_b, and e_c are phase back-EMFs. ω_m is a mechanical angular velocity.

Fig. 2 shows that the torque ripple can be minimized and the stable control is achieved when the phase current with square wave form is injected into the part where the magnitude of back-EMFs is fixed.

3. PROPOSED SENSORLESS CONTROL METHOD

The proposed sensorless control method is based on the fact that the rotor position can be detected by using a trapezoidal back-EMF of BLDC motors. Since a back-EMF of the BLDC motor is not measured directly, it is estimated by the unknown input observer. This unknown input observer is constructed by a back-EMF regarded as an unknown input and state of the BLDC motor drive system. The sensorless control method using the unknown input observer can be obtained as follows:

3.1. First Line-to line back-EMF estimation using the unknown input observer

Since the neutral point of the BLDC motor is not offered, it is difficult to construct the equation for one phase. Therefore, the unknown input observer is considered by the following line-to-line equation:

$$\dot{i}_{ab} = -\frac{2R_s}{2L} i_{ab} + \frac{1}{2L} v_{ab} - \frac{1}{2L} e_{ab}. \tag{3}$$

In (3), i_{ab} and v_{ab} can be measured, therefore they are "known" state variables. On the other hand, since e_{ab} cannot be measured, this term is considered as an

"unknown" state. The equation (3) can be rewritten in the following matrix form:

$$\dot{\mathbf{x}} = \mathbf{A}\mathbf{x} + \mathbf{B}\mathbf{u} + \mathbf{F}\mathbf{w}, \tag{4}$$

$$\mathbf{y} = \mathbf{C}\mathbf{x}, \tag{5}$$

where

$$\mathbf{A} = \left[-\frac{2R_s}{2L}\right], \mathbf{B} = \left[\frac{1}{2L}\right], \mathbf{F} = \left[-\frac{1}{2L}\right],$$

$$\mathbf{x} = [i_{ab}], \mathbf{u} = [v_{ab}], \mathbf{w} = [e_{ab}], \mathbf{y} = [i_{ab}], \mathbf{C} = [1].$$

The back-EMF is regarded as an unknown disturbance (4). Even unknown disturbances are difficult to presuppose, these disturbances mostly has one form of step, ramp, or trigonometrical function. Therefore, unknown disturbances can be represented by a differential equation:

$$\dot{\mathbf{z}} = \mathbf{D}\mathbf{z}, \tag{6}$$

$$\mathbf{w} = \mathbf{H}\mathbf{z}, \tag{7}$$

where

$$\mathbf{D} = \begin{bmatrix} 0_{(\delta-1)\times 1} & \mathbf{I}_{(\delta-1)} \\ 0_{1\times 1} & 0_{1\times(\delta-1)} \end{bmatrix}, \mathbf{H} = \begin{bmatrix} \mathbf{I}_1 & 0_{1\times(\delta-1)} \end{bmatrix}.$$

I is identity matrix, and δ is degree of polynomial expression under:

$$\mathbf{w} = \sum_{i=0}^{\delta} a_i t^i, \quad \delta \geq 1, \tag{8}$$

where a_i denotes a set of unknown coefficient vectors. In cases of no experimental information about disturbance, a_i can be defined as $a_i = 0$ in (8). This modelling method offers an effective model about most disturbances as well as unknown disturbances that change slowly by increasing the degree of polynomial expression. Henceforth it is assumed without loss of generality that the unknown disturbance w is modelled by the general completely observable dynamical system of (6, 7). Therefore, the entire system can be expressed by the augmented equation that introduces disturbances of differential equation form modelling the back-EMF. The augmented model can be shown as (9) and (10):

$$\dot{\mathbf{x}}_a = \mathbf{A}_a\mathbf{x}_a + \mathbf{B}_a\mathbf{u}, \tag{9}$$

$$\mathbf{y} = \mathbf{C}_a\mathbf{x}_a, \tag{10}$$

where

$$\mathbf{A}_a = \begin{bmatrix} \mathbf{A} & \mathbf{FH} \\ 0 & \mathbf{E} \end{bmatrix} = \begin{bmatrix} -\frac{2R_s}{2L} & -\frac{1}{2L} \\ 0 & 0 \end{bmatrix}, \mathbf{x}_a = \begin{bmatrix} i_{ab} \\ e_{ab} \end{bmatrix},$$

$$\mathbf{B}_a = \begin{bmatrix} \mathbf{B} \\ 0 \end{bmatrix} = \begin{bmatrix} \frac{1}{2L} \\ 0 \end{bmatrix}, \mathbf{u} = [v_{ab}], \mathbf{y} = [i_{ab}],$$

$$\mathbf{C}_a = \begin{bmatrix} \mathbf{C} & 0 \end{bmatrix} = \begin{bmatrix} 1 & 0 \end{bmatrix},$$

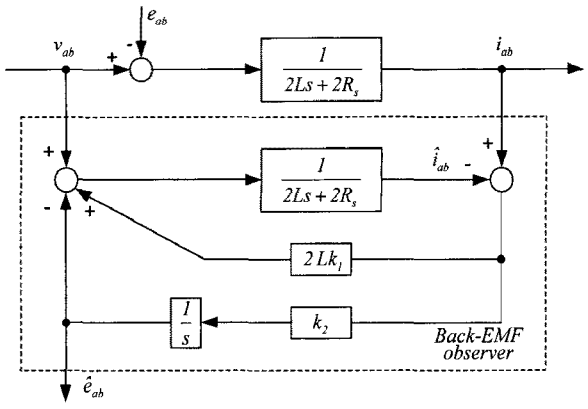

Fig. 3. Block diagram of the proposed back-EMF observer.

and the degree of polynomial expression for disturbance is established by $\delta = 1$.

Since systems of (9) and (10) are observable, it is possible to compose the following observer:

$$\dot{\hat{\mathbf{x}}}_a = \mathbf{A}_a\hat{\mathbf{x}}_a + \mathbf{B}_a\mathbf{u} + \mathbf{K}(\mathbf{y} - \hat{\mathbf{y}}). \tag{11}$$

K is the gain matrix of the observer [19]. If the gain of the observer is selected properly, this observer can accurately estimate line-to-line currents and back-EMFs of motors. Fig. 3 shows a block diagram of the proposed back-EMF observer.

Therefore, the equation of whole observer including all of three phases is as follows:

$$\frac{d}{dt}\begin{bmatrix} \hat{i}ab \\ \hat{e}ab \\ \hat{i}bc \\ \hat{e}bc \\ \hat{i}ca \\ \hat{e}ca \end{bmatrix} = \begin{bmatrix} -\frac{2Rs}{2L} & -\frac{1}{2L} & 0 & 0 & 0 & 0 \\ 0 & 0 & 0 & 0 & 0 & 0 \\ 0 & 0 & -\frac{2Rs}{2L} & -\frac{1}{2L} & 0 & 0 \\ 0 & 0 & 0 & 0 & 0 & 0 \\ 0 & 0 & 0 & 0 & -\frac{2Rs}{2L} & -\frac{1}{2L} \\ 0 & 0 & 0 & 0 & 0 & 0 \end{bmatrix} \begin{bmatrix} \hat{i}ab \\ \hat{e}ab \\ \hat{i}bc \\ \hat{e}bc \\ \hat{i}ca \\ \hat{e}ca \end{bmatrix}$$

$$+ \begin{bmatrix} \frac{1}{2L} & 0 & 0 \\ 0 & 0 & 0 \\ 0 & \frac{1}{2L} & 0 \\ 0 & 0 & 0 \\ 0 & 0 & \frac{1}{2L} \\ 0 & 0 & 0 \end{bmatrix} \begin{bmatrix} vab \\ vbc \\ vca \end{bmatrix} + \begin{bmatrix} k1 & 0 & 0 \\ k2 & 0 & 0 \\ 0 & k3 & 0 \\ 0 & k4 & 0 \\ 0 & 0 & k5 \\ 0 & 0 & k6 \end{bmatrix} \begin{bmatrix} iab - \hat{i}ab \\ ibc - \hat{i}bc \\ ica - \hat{i}ca \end{bmatrix}. \tag{12}$$

3.2. Commutation function

The sensorless control method that decides commutation instances of switching devices by detecting ZCP of back-EMF has been commonly used. However, this method cannot detect ZCP at a low-

speed range. In order to solve this problem, the sensitive commutation function defined by using the line-to-line back-EMF observer is proposed to improve the performance of the sensorless control scheme as shown in Fig. 4 and the commutation functions (CF) are defined as below:

$$\text{Mode 1 and 4: } CF(\theta)_1 = \frac{\hat{e}_{bc}}{\hat{e}_{ca}}, \tag{13}$$

$$\text{Mode 2 and 5: } CF(\theta)_2 = \frac{\hat{e}_{ab}}{\hat{e}_{bc}}, \tag{14}$$

$$\text{Mode 3 and 6: } CF(\theta)_3 = \frac{\hat{e}_{ca}}{\hat{e}_{ab}}. \tag{15}$$

As shown in Fig. 4, the commutation function for the mode conversion from mode 6 to 1 is represented by the fractional equation consisted of the numerator ($\hat{e}_{bc}$) having a constant negative magnitude and the gradually decreasing denominator ($\hat{e}_{ca}$). Before mode change, this commutation function instantaneously changes from negative infinity to positive infinity and this moment is considered as the position signal so that this feature can be certainly distinguished from noises by selecting a relevant threshold magnitude. Although a similar commutation function has been reported [20], the commutation functions of the proposed scheme have the characteristic of less noise sensitive.

Figs. 5 and 6 represent the proposed commutation function and the existing commutation function, respectively. In Fig. 5, the lower noise ① than threshold (th) 1 dose not affect position detection of the rotor, however, the bigger noise ② than th 1 can be regarded as commutation signal and generate error of a rotor position. Also, in case of commutation function such as ③ due to variation of back-EMF, the th voltage level should be increased to achieve the exact commutation signal, as in case the noise ② exists.

On the other hand, as shown in Fig. 6, the bigger

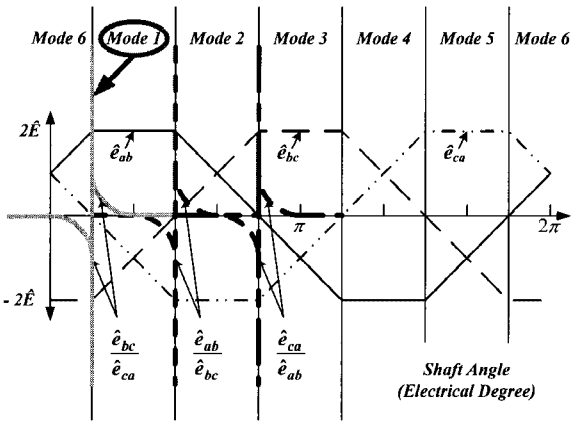

Fig. 4. Proposed commutation functions.

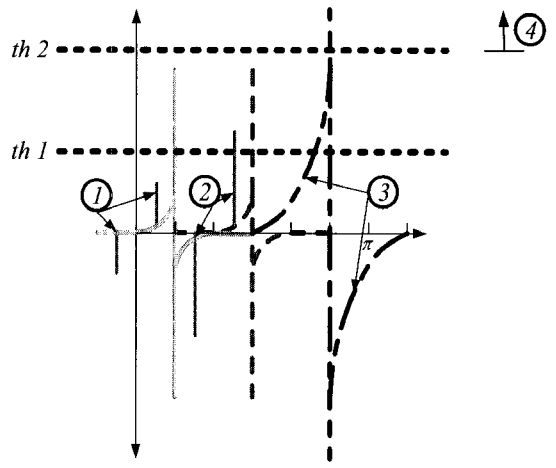

Fig. 5. Commutation function using the existing method.

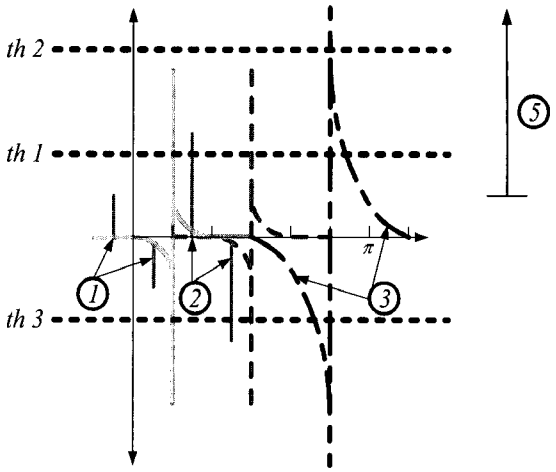

Fig. 6. Commutation function using the proposed method.

signal than th 1 or th 3, such as ② and ③, are not regarded as commutation signal in the proposed method since it is generated in the point before negative infinity, namely, the signal after passing negative infinity (th 3) and satisfying the bigger magnitude than th 1 is regarded as the commutation signal. Finally, the existed method is sensitive to the noise, and the calculation of commutation point can be delayed because it should select the bigger voltage level th than th 2 (④). But the proposed method can generate the exact position information in the lower th voltage level as ⑤.

3.3. The estimation of speed and position

If the estimated magnitude of a back-EMF is defined, the rotor position and the speed can be calculated by simple arithmetic. The relationship between the speed and the magnitude of a back-EMF in BLDC motors is:

$$E = K_e \omega_e, \tag{16}$$

where E is a back-EMF magnitude, K_e is a back-

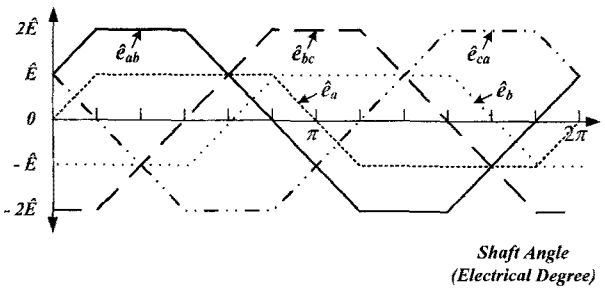

Fig. 7. Relation between the estimated line-to-line back-EMFs and the estimated back-EMFs.

EMF constant, and ω_e is an electrical angular velocity.

As shown in Fig. 7, the magnitude of the back-EMF is estimated by the maximum magnitude of the line-to-line back-EMF that the unknown input observer offers. Therefore, the speed can be calculated by using the estimated magnitude of the back-EMF as follows:

$$\hat{\omega}_e = \frac{\hat{E}}{K_e}, \tag{17}$$

$$\hat{\omega}_m = \frac{2}{P}\hat{\omega}_e, \tag{18}$$

where $\hat{\omega}m$ is an estimated mechanical angular velocity and P is the number of poles.

The rotor position is obtained by integrating the motor speed:

$$\hat{\theta} = \int \hat{\omega}_e dt + \theta_0, \tag{19}$$

where θ_0 is the initial position of rotor.

3.4. Starting procedure

It is necessary to have the process start up in sensorless control because it has difficulty detecting the rotor position at standstill. The simple 'align and go' scheme [3], which is a widely used method in commercialized BLDC sensorless controller, has been adopted for the starting procedure for the proposed scheme. In this method, the controller aligns the rotor with a predetermined position by conducting two phases of a motor before rotations, and then rotates the rotor according to a given switching sequence with incensement of the rotor speed. In conventional sensorless methods such as detecting the ZCP of terminal voltages, the closed loop control starts from a relatively high speed, since they need a high speed enough to achieve a certain level of voltage signals.

On the contrary, the proposed method can determine the motor position within a 60° motor revolution. Since the proposed method detects the commutation instance by using commutation functions, which are based on estimated line-to-line back-EMFs with 60° resolution and shown in (13-15). After detecting the first commutation point, torque and speed are controlled with a sensorless algorithm with the estimated speed calculated by the time interval of commutation points.

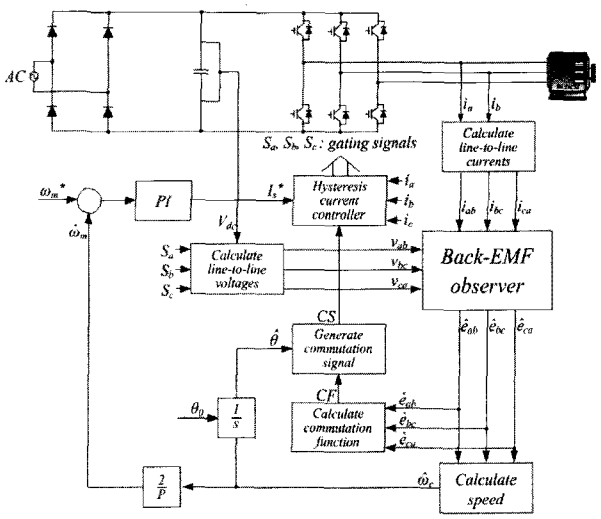

Fig. 8. Overall structure of the proposed sensorless drive system.

3.5. The overall black diagram of the proposed sensorless scheme

Fig. 8 illustrates the overall structure of the proposed sensorless drive system. The line-to-line voltage is calculated based on the DC-link voltage and switching status of the inverter. As described above, the back-EMF observer provides the estimated line-to-line back-EMF (12). The commutation function (13-15), the speed (18), and the rotor position (19) are calculated from the estimated line-to-line back-EMFs. The commutation signal generation block generates commutation signals based on the calculated rotor position and the commutation function. Each phase current is controlled by the hystersis current controller using the commutation signals.

4. SIMULATION RESULTS

Simulations have been performed on the BLDC motor that has the ratings and parameters as shown in Table 1. The Matlab/Simulink environment was used for the simulations.

Table 1. Ratings and parameters of BLDC motor.

Rated voltage	V	310 (V)
Rated torque	T_e	1.5 (Nm)
Rated speed	N_r	1650 (rpm)
Stator resistance	R_s	7.3 (Ω)
Stator inductance	L	0.02 (H)
Rotor inertia	J_m	23.16 ×10^{-4} (kg · m2)
Back-EMF constant	K_e	0.25 (V/rad/ sec)
Number of pole pairs	P_n	2

This paper evaluates the robustness of the sensorless algorithm under variations of speed and load. To test the dynamic behaviour of the drive under load disturbance, we assert a dynamic load of 0.5 Nm and 1.5 Nm to the motor at 2.3 s and 0.9 s while it runs at 50 rpm (Fig. 9) and 1650 rpm (Fig. 10), respectively. As shown in Figs. 9 and 10, the speed drops slightly while the phase current increases to

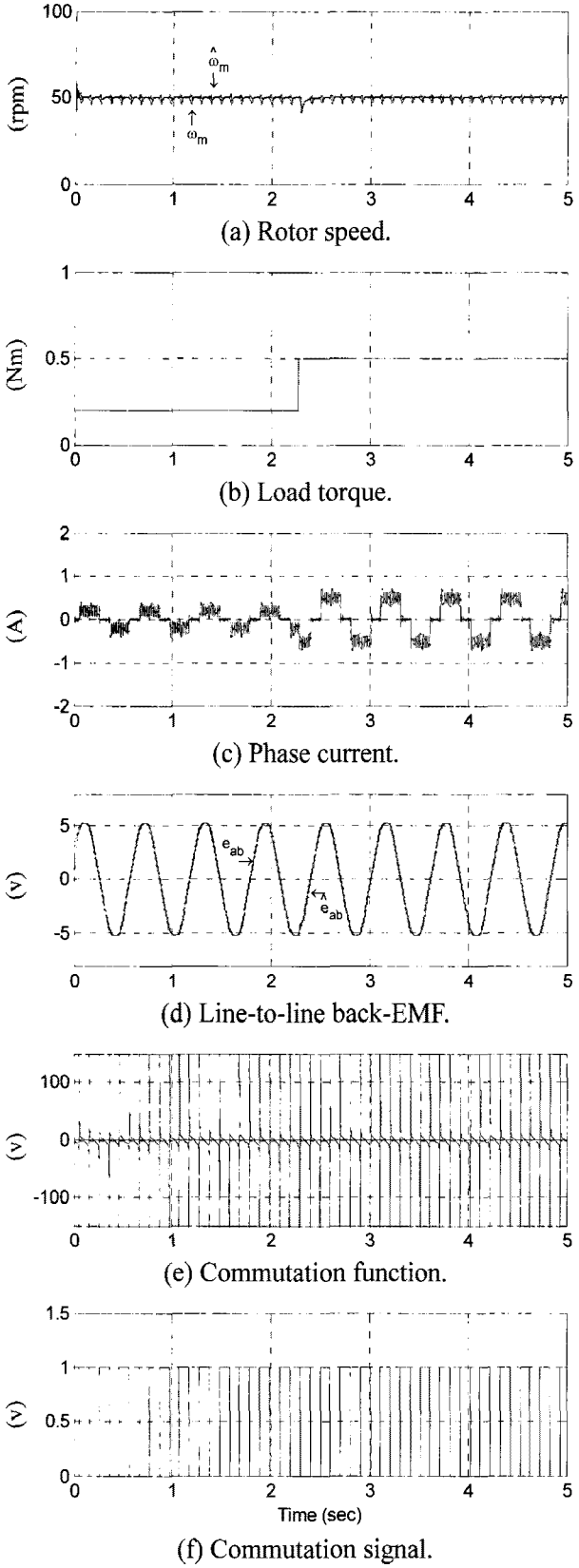

(a) Rotor speed.
(b) Load torque.
(c) Phase current.
(d) Line-to-line back-EMF.
(e) Commutation function.
(f) Commutation signal.

Fig. 9. Response waveforms at under step change of load torque. (Speed reference: 50 rpm, Load: 0.2 → 0.5 Nm).

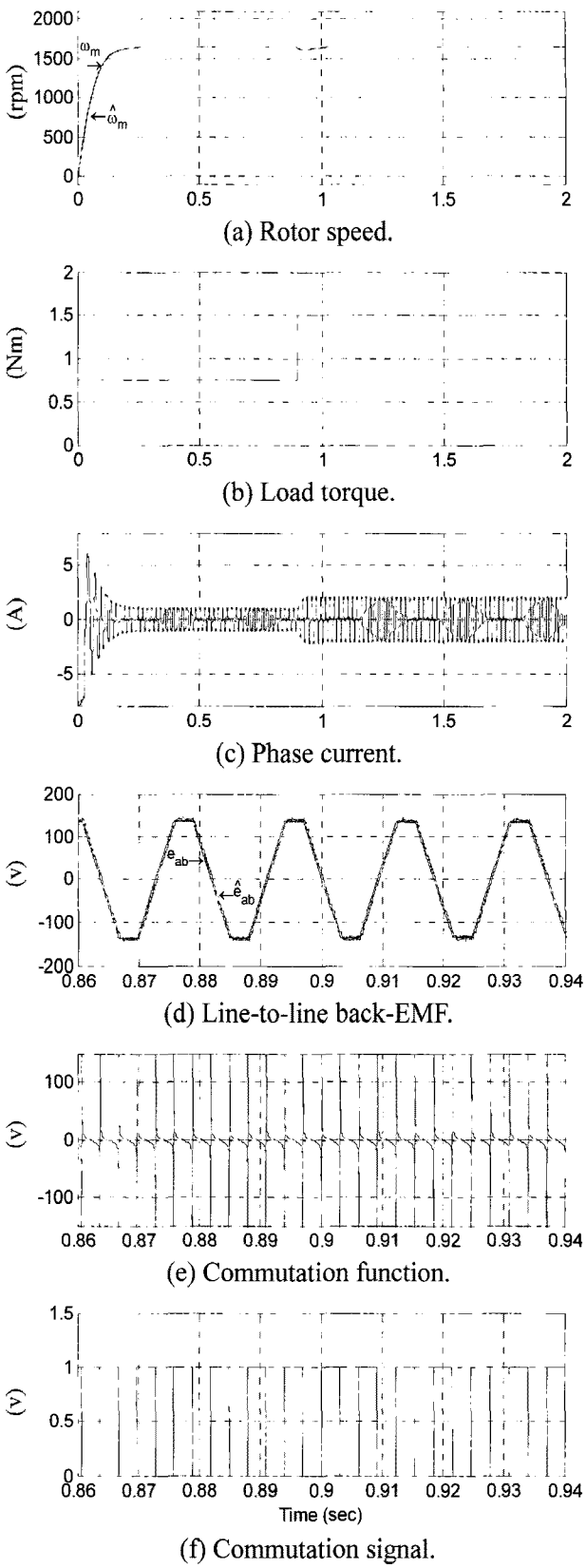

(a) Rotor speed.
(b) Load torque.
(c) Phase current.
(d) Line-to-line back-EMF.
(e) Commutation function.
(f) Commutation signal.

Fig. 10. Response waveforms under step change of load torque. (Speed reference: 1650 rpm, Load: 0.75 → 1.5 Nm).

reject the disturbance. Note also that the estimated speed tracks the actual speed quite well through the transient. In this profile, the commutation signals (Figs. 9(f) and 10(f)) are generated when the magnitude of the commutation function (Figs. 9(e) and 10(e)) is bigger than the threshold magnitude defined by 5 V.

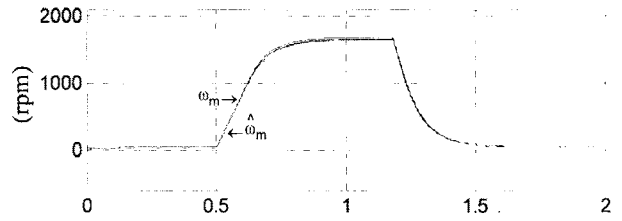

(a) Rotor speed.

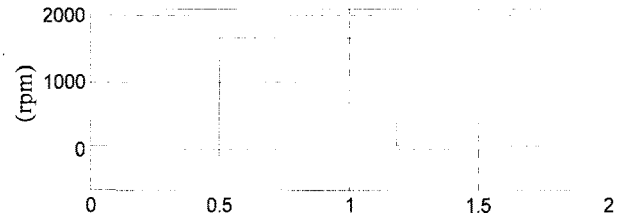

(b) Speed reference.

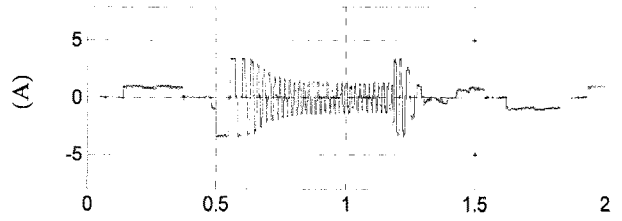

(c) Phase current.

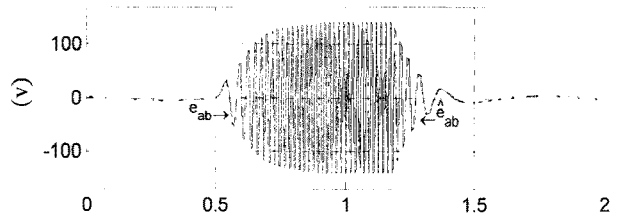

(d) Line-to-line back-EMF.

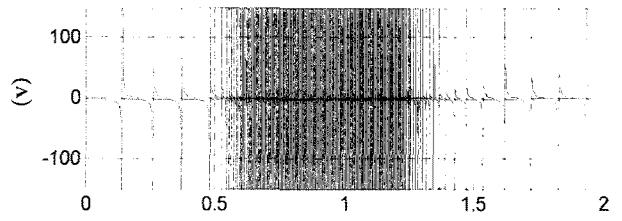

(e) Commutation function.

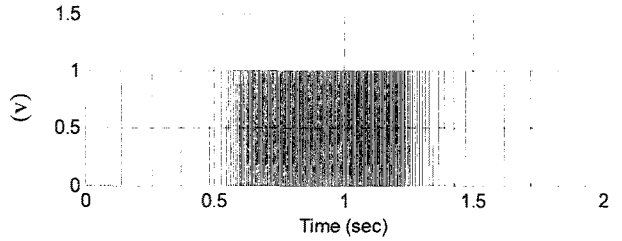

(f) Commutation signal.

Fig. 11. Response waveforms under step change of speed reference. (Load: 0.75 Nm, Speed reference: 50 → 1650 → 50 rpm).

The speed-step response of the proposed sensorless algorithm is shown in Fig. 11. Initially, the machine is running at constant speed of 50 rpm under 1.18 Nm load condition. The speed command is changed instantaneously from 50 to 1650 rpm and back to 50 rpm. It is clearly verified from this test that the proposed sensorless drive algorithm has good transient response under various speed operating conditions.

5. EXPERIMENTAL RESULTS

In order to verify the proposed sensorless control method, experiments were performed by a designed laboratory prototype as shown in Fig. 12. The parameters of the motor model used in the simulations correspond to the parameters of the motor used in the experiments. The main board is composed of the digital signal processor (DSP, TMS320VC33), FPGA, and AD/DA converters. The used power module in experiments is implemented with PM75RLA060 (IPM) devices. The sampling time in the current control algorithm is 50μs. The electric dynamo-meter attached to the machine provides an external load.

The commutation function made by the unknown input observer is shown in Fig. 13. It shows a rigid operation even in a noisy environment since commutation function has the negative magnitude before the commutation point.

The experimental results are depicted in Figs. 14-19. Figs. 14 and 16 show the estimated tracking ability at

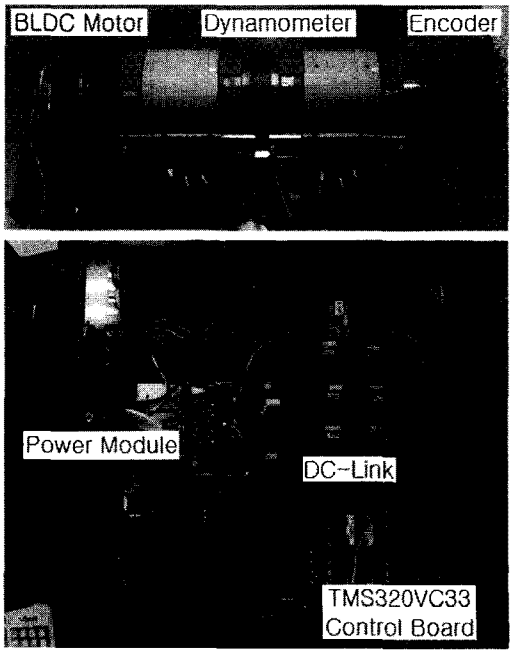

Fig. 12. Laboratory prototype for the experimental verifications.

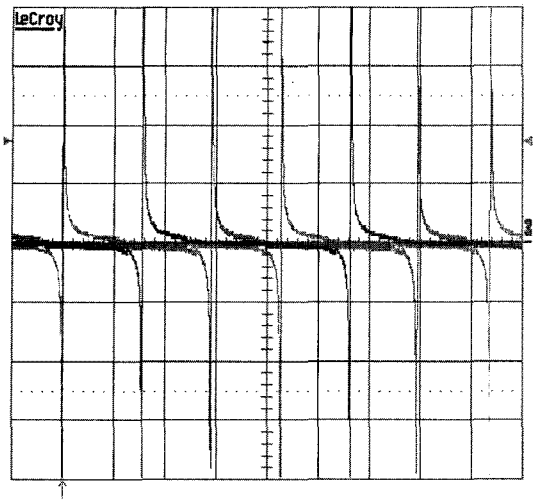

Fig. 13. Experimental result of commutation function. (10 ms/div.)

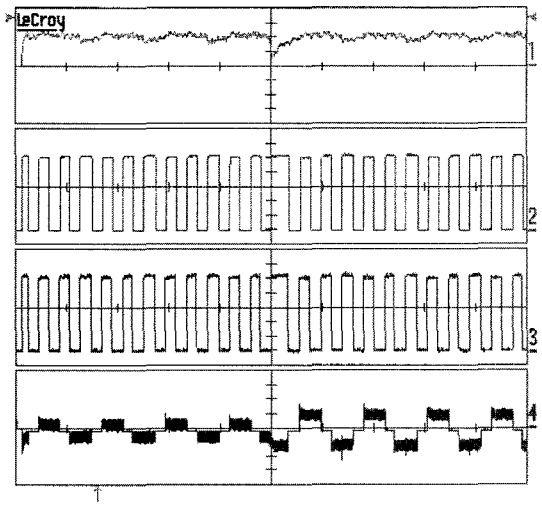

Fig. 14. Response waveforms under step change of load torque. (Speed reference: 50 rpm, Load: 0.2 → 0.5 Nm, 500 ms/div.)
[from top to bottom: Rotor speed (25 rpm/div.); Commutation signal by the proposed method (200mV/div.); Commutation signal by a Hall sensor (200 mV/div.); Phase current (500 mA/div.)]

low (50 rpm) and the high (1650 rpm) speeds under load changes, respectively. It can be seen from Fig. 14, that the rise time of the speed response is about 50 msec and the drive takes about 180 msec to reject the load torque disturbance introduced in the system. In case of Fig. 16, the rise time of the speed response is about 100 msec and the drive takes about 75 msec to reject the load torque disturbance introduced in the system. Figs. 15 and 17 show enlarged waveforms of Figs. 14 and 16. In the following figures, the commutation function and the commutation signal are well synchronized. The Hall signal is compared with the estimated one at a constant speed. As a result, although sensorless control has an error of about 3°

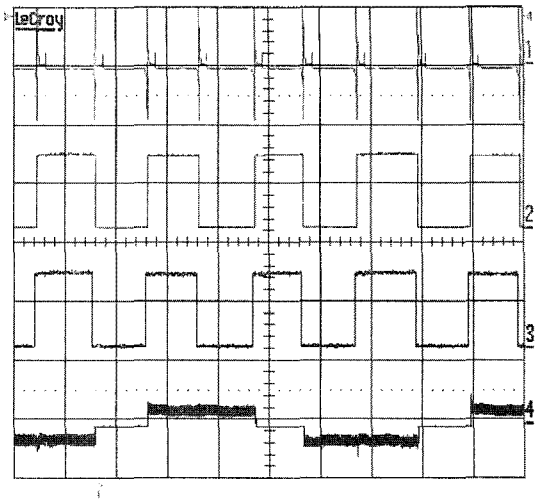

Fig. 15. Enlarged response waveforms under step change of load torque. (Speed reference: 50 rpm, Load: 0.5 Nm, 100 ms/div.)
[from top to bottom: Commutation function (500 mV/div.); Commutation signal by the proposed method (200 mV/div.); Commutation signal by a Hall sensor (200 mV/div.); Phase current (500 mA /div.)]

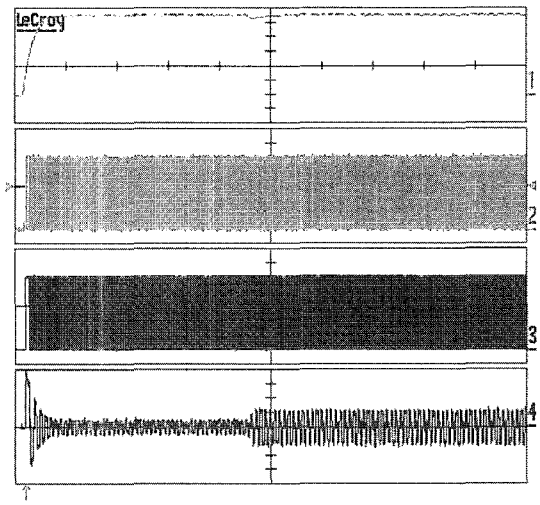

Fig. 16. Response waveforms under step change of load torque. (Speed reference: 1650 rpm, Load: 0.75 → 1.5 Nm, 200 ms/div.)
[from top to bottom: Rotor speed (400 rpm /div.); Commutation signal by the proposed method (200 mV/div.); Commutation signal by a Hall sensor (200 mV/div.); Phase current (2 A/div.)]

and 1.4°, the estimated signal shows good linearity and a satisfactory correspondence to the actual Hall signal that it obtained with the motor built-in a Hall sensor.

The worst commutation angle errors at different speeds based on the experimental results are shown in Fig. 18. To find the value of worst-case at each speed, the motor is operated repeatedly, and the worst

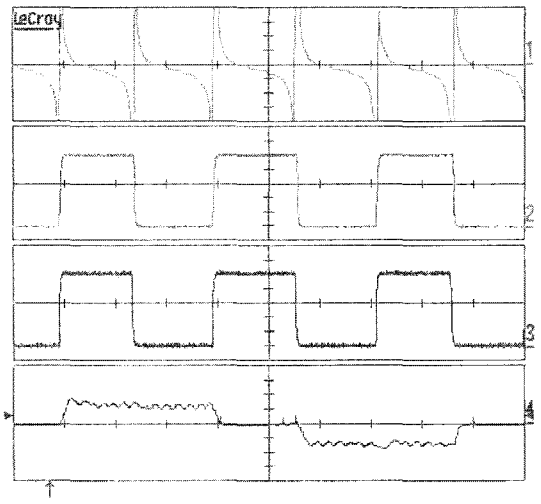

Fig. 17. Enlarged response waveforms under step change of load torque. (Speed reference: 1650 rpm, Load: 0.75 Nm, 2 ms/div.) [from top to bottom: Commutation function (500 mV/div.); Commutation signal by the proposed method (200 mV/div.); Commutation signal by a Hall sensor (200 mV/div.); Phase current (1 A/div.)]

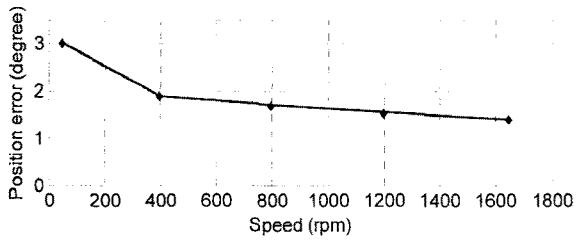

Fig. 18. Worst-Case commutation angle error. (Experimental result)

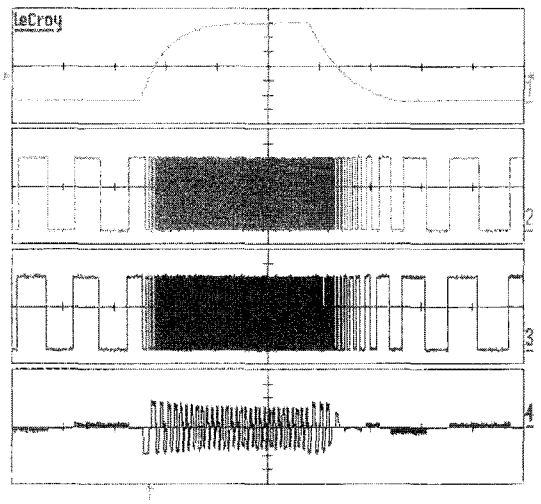

Fig. 19. Response waveforms under step change of speed reference. (Load: 0.75 Nm, Speed reference: 50→1650→ 50 rpm, 200 ms/div.) [from top to bottom: Rotor speed (200 rpm/div.); Commutation signal by the proposed method (200 mV/div.); Commutation signal by a Hall sensor (200 mV/div.); Phase current (1 A/div.)]

commutation angle error is obtained by making a comparison between a commutation signal by the proposed method and a Hall signal. Although a position error increases according to the decrease of the speed, the proposed sensorless control shows a good dynamic response over a full speed operating.

Fig. 19 shows the responses for step change of speed reference. From this experiment, it is seen that the proposed system performs well under such speed changes.

6. CONCLUSIONS

This paper presented a new approach to the sensorless control of the BLDC motor drives using the unknown input observer. This observer can be obtained effectively by using the equation of augmented system and an estimated line-to-line back-EMF that is modelled as an unknown input. As a result, the actual rotor position as well as the machine speed can be estimated strictly even in the transient state from the estimated line-to-line back-EMF.

The novel sensorless method using an unknown input observer can

- be achieved without additional circuits.
- estimate a rotor speed in real time for precise control.
- make a precise commutation pulse even in transient state as well as in steady state.
- detect the rotor position effectively over a full speed range, especially at a low speed range.
- calculate commutation function with a noise insensitive.
- be easily realized for industry application by simple control algorithm.

The simulation and experimental results successfully confirmed the validity of the developed sensorless drive technique using the commutation function.

REFERENCES

[1] N. Matsui, "Sensorless PM brushless DC motor drives," *IEEE Trans. on Industrial Electronics*, vol. 43, no. 2, pp. 300-308, 1996.

[2] K. Xin, Q. Zhan, and J. Luo, "A new simple sensorless control method for switched reluctance motor drives," *KIEE J. Electr. Eng. Technol.*, vol. 1, no. 1, pp. 52-57, 2006.

[3] S. Ogasawara and H. Akagi, "An approach to position sensorless drive for brushless DC motors," *IEEE Trans. on Industry Applications*, vol. 27, no. 5, pp. 928-933, 1991.

[4] J. C. Moreira, "Indirect sensing for rotor flux position of permanent magnet AC motors operating over a wide speed range," *IEEE Trans. on Industry Applications*, vol. 32, no. 6, pp. 1394-1401, 1996.

[5] J. X. Shen, Z. Q. Zhu, and D. Howe, "Sensorless flux-weakening control of permanent-magnet brushless machines using third harmonic back EMF," *IEEE Trans. on Industry Applications*, vol. 40, no. 6, pp. 1629-1636, 2004.
[6] T. M. Jahns, R. C. Becerra, and M. Ehsani, "Integrated current regulation for a brushless ECM drive," *IEEE Trans. on Power Electronics*, vol. 6, no. 1, pp. 118-126, 1991.
[7] H. R. Andersen and J. K. Pedersen, "Sensorless ELBERFELD control of brushless DC motors for energy-optimized variable-speed household refrigerators," *EPE Conf. Rec.*, vol. 1, pp. 314-318, 1997.
[8] G. J. Su and J. W. Mckeever, "Low cost sensorless control of brushless DC motors with improved speed range," *IEEE Trans. on Power Electronics*, vol. 19, pp. 296-302, 2004.
[9] K. Iizuka, H. Uzuhashi, and M. Kano, "Microcomputer control for sensorless brushless motor," *IEEE Trans. on Industry Applications*, vol. 27, pp. 595-601, 1985.
[10] H. G. Yee, C. S. Hong, J. Y. Yoo, H. G. Jang, Y. D. Bae, and Y. S. Park, "Sensorless drive for interior permanent magnet brushless DC motors," *Proc. of IEEE International Conf. on Electric Machines and Drives,* 18-21, pp. TD1/3.1-3.3, 1997.
[11] Q. Jiang, C. Bi, and R. Huang, "A new phase-delay-free method to detect back EMF zero-crossing points for sensorless control of spindle motors," *IEEE Trans. Magn.*, vol. 41, no. 7, pp. 2287-2294, 2005.
[12] A. T. Alexandridis and G. D. Galanos, "Design of an optimal current regulator for weak AC/DC systems using Kalman filtering in the presence of unknown inputs," *Proc. IEE*, vol. 136, no. 2, pp. 57-63, 1989.
[13] M. Saif, "Robust servo design with applications," *Proc. Inst. Elect. Eng.*, vol. 140, no. 2, pp. 87-92, 1993.
[14] M. Aldeen and J. F. Marsh, "Decentralised observer-based control scheme for interconnected dynamical systems with unknown inputs," *Proc. Inst. Elect. Eng.*, vol. 146, no. 5, pp. 349-358, 1999.
[15] T. G. Park, J. S. Ryu, and K. S. Lee, "Actuator fault estimation with disturbance decoupling," *Proc. Inst. Elect. Eng.*, vol. 147, no. 5, pp. 501-508, 2000.
[16] T. G. Park and K. S. Lee, "Process fault isolation for linear systems with unknown inputs," *Proc. Inst. Elect. Eng.*, vol. 151, no. 6, pp. 720-726, 2004.
[17] B. Marx, D. Koenig, and J. Ragot, "Design of observers for Takagi-Sugeno descriptor systems with unknown inputs and application to fault diagnosis," *Proc. Inst. Elect. Tech.*, vol. 1, no. 5, pp. 1487-1495, 2007.
[18] P. Pillay and R. Krishnan, "Modeling, simulation, and analysis of permanent-magnet motor drives, part II: The bruahless DC motor drive," *IEEE Trans. on Industry Applications*, vol. 25, no. 2, pp. 274-279, 1989.
[19] S. H. Huh, S. J. Seo, I. Choy, and G. T. Park, "Design of a robust stable flux observer for induction motors," *KIEE J. Electr. Eng. Technol.*, vol. 2, no. 2, pp. 280-285, 2007.
[20] T. H. Kim and M. Ehasani, "Sensorless control of the BLDC motors from near-zero to high speeds," *IEEE Trans. on Power Electronics*, vol. 19, no. 6, pp. 1635-1645, 2004.

Tae-Sung Kim received the M.S. degree in Electrical Engineering from Hanyang University, Seoul, Korea, in 2002, where he is currently working toward a Ph.D. degree. His research interests include power electronics, sensorless control for brushless dc motor, fault tolerant control methods, and electric wheelchair control.

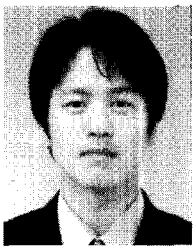

Byoung-Gun Park received the B.S. in Electrical Engineering from Myongji University, Yongin, Korea, in 2005 and M.S. degrees in Electrical Engineering from Hanyang University, Seoul, Korea, in 2007, where he is currently working toward a Ph.D. degree. His research interests include variable speed drives and power converter for high-speed train.

Dong-Myung Lee received the B.S. and M.S. degrees in Electrical Engineering from Hanyang University, Seoul, Korea, in 1994 and 1996, respectively, and the Ph.D. degree in Electrical and Computer Engineering from the Georgia Institute of Technology, Atlanta, in 2004. From 1996 to 2000, he worked in the LG Electronics Inc., Seoul, Korea. From 2004 to 2007, he was employed by the Samsung SDI R&D Center, Yongin, Korea, as a Senior Engineer. From 2007 to 2008, he was with the Department of Electrical Engineering, Hanyang University, as a Research Professor. Since 2008, he has been the Faculty of the School of Electronics and Electrical Engineering at Hongik University, Seoul, Korea. His research interests and experience include variable speed drives, power quality compensation devices, and driving systems for large size display panels.

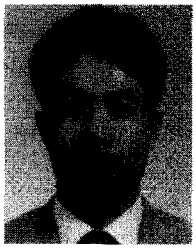

Ji-Su Ryu received the M.S. and Ph.D. degrees in Electrical Engineering from Dankook University, Seoul, Korea, in 1996 and 2002, respectively. From 2004 to 2005, he was a Research Professor with the Department of Electrical Engineering, Hanyang University. Since 2006, he has been with Hanyoung Electrical Industry Company, where he is a Director of R&D center. His main research interests are motor drives, uninterruptible power supplies, and fault tolerant control methods.

Dong-Seok Hyun received the B.S. and M.S. degrees in Electrical Engineering from Hanyang University, Seoul, Korea, in 1973 and 1978, respectively, and the Ph.D. degree in Electrical Engineering from Seoul National University, Seoul, Korea, in 1986. From 1976 to 1979, he was with the Agency for Defense Development, Daejeon, Korea, as a Researcher. From 1984 to 1985, he was a Research Associate in the Department of Electrical Engineering, University of Toledo, Toledo, OH. From 1988 to 1989, he was a Visiting Professor in the Department of Electrical Engineering, Technical University of Munich, Germany. Since 1979, he has been with Hanyang University, where he is currently a Professor in the Department of Electrical Engineering and the Director of the Advanced Institute of Electrical Engineering and Electronics (AIEE). He is the author of more than 120 publications concerning electric machine design, high-power engineering, power electronics, and motor drives. His research interests include power electronics, motor drives, digital signal processing, traction, and their control systems. Dr. Hyun is a Member of the IEEE Power Electronics, IEEE Industrial Electronics, IEEE Industry Applications, and IEEE Electron Devices Societies. He is also a Member of the Institution of Electrical Engineers, U.K., the Korean Institute of Power Electronics, Seoul, and the Korean Institute of Electrical Engineers, Seoul.